INTERNATIONAL JOURNAL OF OPTIMIZATION IN CIVIL ENGINEERING
Int. J. Optim. Civil Eng., 2024; 14(4):503-537

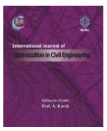

OPTIMAL DESIGN OF REGULAR DIAGRID SYSTEMS WITH DISCRETE VARIABLES UNDER DIFFERENT GEOMETRIES AND BOUNDARY CONDITIONS

L. Coelho[1], M. Shahrouzi[2*, †], and N. Khavaninzadeh[2]
[1]*Graduate Program in Electrical Engineering, Federal University of Parana, Curitiba, PR, Brazil*
[2]*Civil Engineering Department, Faculty of Engineering, Kharazmi University, Tehran, Iran*

[DOI: 10.22068/ijoce.2024.14.4.605]

ABSTRACT

Diagrids are of practical interest in high-rise buildings due to their architectural configuration and efficiency in withstanding lateral loads by exterior diagonal members. In the present work, diagrid models are screened based on a sizing optimization approach. Section index of each member group is treated as a discrete design variable in the optimization problem to be solved. The structural constraints are evaluated due to Load and Resistant Design Factor regulations under both gravitational and wind loadings. The research is threefold: first, falcon optimization algorithm is utilized as a meta-heuristic paradigm for such a large-scale and highly constrained discrete problem. Second, the effect of geometry variation in diagrids on minimal structural weight is studied for 18 diagrid models via three different heights (12, 20 and 30 stories) and three diagrid angles. Third, distinct cases of rigid and flexible bases are compared to study the effect of such boundary conditions on the results. The effect of soil flexibility beneath the foundation on the optimal design was found highly dependent on the diagrid geometry. The best weight and performance in most of the treated examples belong to the geometry that covers two stories by every grid line on the flexible-base.

Keywords: Tall Building; Diagrid Layout; Discrete Constrained Optimization; Meta-heuristic Algorithm.

Received: 3 September 2024; Accepted: 8 October 2024

[*]Corresponding author: Civil Engineering Department, Faculty of Engineering, Kharazmi University, Tehran, Iran
[†]E-mail address: shahruzi@khu.ac.ir (Mohsen Shahrouzi)

1. INTRODUCTION

High-rise buildings are desired to resist gravitational and lateral loadings and confine story sways within acceptable limits. Diagrids are efficient solutions for tall buildings among various configurations of lateral-resisting systems [1]. A diagrid consists of strong diagonal bracings in premiere frames with or without exterior columns [2,3]. Sizing design of diagrid members can alter distribution of internal forces and other structural responses. Every such design that satisfies code-based regulations is considered feasible; however, optimization is employed to select some among these solutions so that cost of material consumption is minimized, as well.

In common practice, member cross sections are selected from a prescribed list of structural profiles. Special consideration should be paid to dealing with such a discrete problem. In this regard, proper representation of design variables is addressed by direct index coding when evolutionary algorithms are applied [4–7]. However, some other meta-heuristic algorithms fall in the category of directional search methods that generate continuous positions during their search [8–12]. Consequently, the resulting design vectors should be rounded to section indices and decoded to the structural models. In this category, many algorithms can be addressed including Genetic Algorithms [13–15], Particle Swarm Optimization [16], Charged System Search [17], Ant Colony Optimization [18–20], Dolphin Echolocation Algorithm [21,22], Bat algorithm [23], Water Evaporation Optimization [24], Vibrating Particles System [25], Coyote Optimization Algorithm [26], Salp Swarm Algorithm [27], Falcon Optimization Algorithm [28], Shuffled Shepherd optimization [29,30] and Escaping Bird Search[31].

A number of investigators have already studied design of diagrid systems. Shahrouzi et al. approached the diagrid design under wind-loading by different optimizers including *Harmony Search* [32,33], *Particle Swarm Optimization* [16,34] and *Mine Blast Algorithm* [35]. The authors presented coding schemes for sizing only and also for simultaneous sizing and layout optimization of diagrids. Gerasimidis [36] proposed a simple approach to optimize size of diagonal members in tall buildings subject to lateral stiffness and deflection constraints. Tomei [37] utilized an encoding scheme for minimal weight design of irregular diagrid structures by genetic algorithms imposing constraints on the lateral stiffness. A lattice-based algorithm is offered by [38] for conceptual design of diagrids. Some investigators studied various diagrid geometries using simplified design of diagrid modules [2,39]. It is while design of frame members affects the design and behavior of diagonal members due to redistribution of internal forces.

The aforementioned works studied behavior of diagrid systems on rigid supports; however, the soil beneath the foundation is actually flexible. The present study simulates the effect of flexible-base by equivalent springs in the structural model. A variant of FOA is then utilized for discrete sizing design of diagrid structures on both rigid and flexible supports to investigate the corresponding structural weights. All diagonal and frame members (beams and columns) contribute in such a sizing design. As another issue, the effect of variation in the diagrid geometry is studied after screening the designs via sizing optimization. It has already been addressed in some literature works by comparative study on structural responses after preliminary design of its members [2]. However, the present study applies FOA to find optimum sections for each uniform grid angle. Symmetric

[DOI: 10.22068/ijoce.2024.14.4.605]

grouping of structural members is employed to deserve practicality of designs as well as to provide computational efficiency via the encoding method.

The rest of this article is structured as follows: The sizing optimization problem and the employed decoding scheme are explained in Section 2. The inspiration concepts and implementation steps of falcon optimization algorithm are reviewed in Section 3. Section 4 introduces loading, boundary conditions and modeling of the structural examples followed by the optimization results. The present work is concluded reporting the most important outcomes in design of regular diagrids.

2. FORMULATION AND ENCODING SCHEME FOR DISCRETE SIZING DESIGN OF DIAGRIDS

It is desired here to minimize the weight of constructional steel material in the entire diagrid system (including diagonals and frame members) provided that the design code requirements are satisfied. The row objective function is given by the following relation:

$$W = \rho \sum_{j=1}^{D} \sum_{i=1}^{N_m(j)} A_i l_i \tag{1}$$

The total weight of a structure;W is calculated using ρ as the material density,l_i as the i^{th} member length and A_i as its cross-sectional area. Every j^{th} design variable is taken the section index of the j^{th} member group. The number of elements in a typical j^{th} group is denoted by$N_m(j)$.

The following side constraints limit the section indices to fall within a prescribed integer set between X_j^L and X_j^U ; referring the available list of structural profiles where:

$$X_j \in \{X_j^L, X_j^L + 1, \dots, X_j^U\}, j = 1,2, \dots, D \tag{2}$$

For practical sizing of diagrids, a discrete set of structural sections is used. Therefore, the aforementioned FOA is specialized by the following encoding actions:

- Any design vector X consists of integer components X_j; denoting an index in the structural section list. Different member types (columns, beams or diagonals) can be associated with different ranges of indices in such a list.
- At the first iteration, initial values for each individual are randomly picked from integers between $X_j^L$and X_j^U.
- The candidate solution of Eq.(7) should be rounded to integer values prior to be decoded into the corresponding sections in the structural model for fitness evaluation.

All behavior constraints are handled by exterior penalty approach of the typical relation:

$$Max\ Fitness\ (X) = -Cost\ (X) \tag{3}$$

$$Cost(X) = W(X) \times \left[1 + k_p \sum \max\left(0, g(X)\right)\right] \tag{4}$$

where each e^{th} inequality constraint is in the standard form of $g_e(X) \leq 0$ and stands k_p for

[DOI: 10.22068/ijoce.2024.14.4.605]

the penalty factor. The constraints are specifically described as follows. $Cost\ (X)$ is a scalar function of the design vector *X*. It denotes the penalized weight derived from raw structural weight *W*. The behavior constraints are applied due to *Load and Resistant Factor Design* (LRFD) procedure of common codes [40,41].

The function $g(X)$ is the allowable stress constraints defined as follows:

$$g_e^q(X) = Sr_e^q - 1 \leq 0 \qquad e = 1,2,\dots,N_m \tag{5}$$

The absolute combined stress ratio, Sr_e^q, is calculated for every e^{th} element in the q^{th} behavior mode given by the design relations as follows:

2.1.1 Axial Behavior

For the compression and tension member the demand to capacity (stress) ratio is calculated as Sr_e^{Axial} by:

$$Sr_e^{Axial} = \frac{P_u}{P_c} \tag{6}$$

$$P_c = \varphi_c P_n = \varphi_c F_{Cr} A_g \tag{7}$$

where $P_u$is the absolute axial response force in the element with a nominal axial strength of P_n. According to LRFD regulations, the corresponding reduction factorφ_c is equal to 0.9. The parameter $A_g$is the gross section area of the element. The critical compressive stress due to elastic buckling F_{Cr}, is given by the design code [40] in term of the slenderness ratio, λ, the yield stress $F_y$and the Euler stress $F_e = \frac{\pi^2 E}{\lambda^2}$.The elasticity modulus of the construction steel material is denoted by E.

L, the effective length factor of *k* and the minimum gyration radius of r_{min}, the slenderness ratio is calculated as $\lambda = \frac{kL}{r_{min}}$.

2.1.2 Combined Behavior

For the members in bending and axial stress the combined stress ratio Sr^{Axial}, is given by the design code [40] as:

$$\frac{P_u}{P_c} \geq 0.2 \Rightarrow \qquad Sr^{Axial} = \frac{P_u}{P_c} + \frac{8}{9}\left(\frac{M_{ux}}{M_{cx}} + \frac{M_{uy}}{M_{cy}}\right) \leq 1 \tag{8}$$

$$\frac{P_u}{P_c} < 0.2 \Rightarrow \qquad Sr^{Axial} = \frac{P_u}{2P_c} + \left(\frac{M_{ux}}{M_{cx}} + \frac{M_{uy}}{M_{cy}}\right) \leq 1$$

where $M_c = \varphi_b M_n$ is the design flexural strength where$M_n$stands for the nominal bending capacity and $\varphi_b = 0.9$ is the corresponding reduction factor. The bending stress ratio is distinctly evaluated in principal axes of the member section based on its shape.

[DOI: 10.22068/ijoce.2024.14.4.605]

2.1.3 Flexural Members: I-Shaped Sections

For cross sections of I-shapes, the nominal bending capacity about major and minor axes are given by M_{nx} and M_{ny} , respectively.

$$M_{nx} = min\{M_{nx1}, M_{nx2}, M_{nx3}, M_{nx4}\} \tag{9}$$

$$M_{ny} = min\{M_{ny1}, M_{ny2}\} \tag{10}$$

The corresponding nominal strengths are given by following relations:

$$M_{nx1} = R_{pg} F_y S_{xc} \tag{11}$$

$$M_{nx2} = \begin{cases} M_{nx1} & L_b \le L_P \\ R_{pg} F_{cr} S_{xc} & L_b > L_P \end{cases} \tag{12}$$

According to the above equations, critical stress F_{cr}due to the lateral-torsional buckling is checked based on the unbraced length of the beam L_b. The parameters $R_{pg}, C_b, L_p, L_r$are given by the design code [40].

$$M_{nx3} = \begin{cases} M_{nx1} & \dfrac{b}{t} \le \lambda_{pf} \\ R_{pg} F_{cr} S_{xc} & \dfrac{b}{t} > \lambda_{pf} \end{cases} \tag{13}$$

In which F_{cr} counts for the local buckling effect based on comparison of the flange slenderness ratio $\lambda = \frac{b_{fc}}{2t_{fc}}$ with its limiting values $\lambda_{pf} = 0.38\sqrt{\frac{E}{F_y}}$ and $\lambda_{rf} = \sqrt{\frac{E}{F_y}}$. b_{fc} is the compressive flange width and t_{fc} is its thickness. S_{xc} and S_{xt} stands for the elastic-section modulus relative to the compressive and tensile flanges, respectively. For symmetric sections:

$$M_{nx4} = F_y S_{xt} \tag{14}$$

For bending action about the minor axis:

$$M_{ny1} = min\{F_y Z_y, 1.6 F_y S_y\} \tag{15}$$

where $S_y$and Z_y denote the elastic and plastic section modulus about the minor axis, respectively.

The nominal bending strength about the minor axis is also checked due to local buckling

[DOI: 10.22068/ijoce.2024.14.4.605]

by:

$$M_{ny2} = \begin{cases} M_{ny1} & \frac{b}{t} \le \lambda_{pf} \\ M_{ny1} - \left(M_{ny1} - 0.7F_y S_y\right)\left(\frac{\lambda - \lambda_{pf}}{\lambda_{rf} - \lambda_{pf}}\right) & \frac{b}{t} > \lambda_{pf} \end{cases} \quad (16)$$

where b and h denote the unconfined parts of the flange and web, respectively.

2.1.4 Flexural Members: Box-Shaped Sections

For cross sections of symmetric Box-shape, the nominal bending capacity is given by:

$$M_n = min\{M_{n1}, M_{n2}, M_{n3}\} \quad (17)$$

$$M_{n1} = F_z Z \quad (18)$$

$$M_{n2} = \begin{cases} M_{n1} & \frac{b}{t_f} \le 1.12\sqrt{\frac{E}{F_y}} \\ M_{n1} - \left(M_{n1} - F_y S\right)\left[3.57\frac{b}{t_f}\sqrt{\frac{F_y}{E}} - 4\right] \le M_{n1} & \frac{b}{t_f} > 1.12\sqrt{\frac{E}{F_y}} \end{cases} \quad (19)$$

$$M_{n3} = \begin{cases} M_{n1} & \frac{h}{t_w} \le 5.7\sqrt{\frac{E}{F_y}} \\ M_{n1} - \left(M_{n1} - F_y S\right)\left[0.305\frac{h}{t_w}\sqrt{\frac{E}{F_y}} - 0.738\right] \le M_{n1} & \frac{h}{t_w} > 5.7\sqrt{\frac{E}{F_y}} \end{cases} \quad (20)$$

where S and Z stand for the elastic and plastic section moduli about the bending axis, respectively.

2.2 Shear Strength Control

For the members in bending the shear stress ratio should also be checked via the following relation:

$$Sr^{Shear} = \frac{V_u}{\varphi V_n} \quad (21)$$

where V_n stands for the nominal shear strength calculated using the web area and the yield stress due to the design code regulations [40]. For the employed sections, the shear strength reduction factor is $\varphi_v = 0{,}9$. The following constraint is then checked for

[DOI: 10.22068/ijoce.2024.14.4.605]

combination of flexural, axial and shear actions:

$$max\{Sr_e^{AxiFlex}, Sr_e^{shear}\} - 1 \leq 0 \tag{22}$$

2.3 Torsional Behavior

For the members in torsion the design strength T_c and the reduction factor φ_T are implemented as:

$$T_c = \varphi_T T_n \tag{23}$$

The corresponding nominal strength in torsion T_n , is given by:

$$T_n = F_{cr} C \tag{24}$$

Then taking the critical stressF_{cr} and the factor C from the design code relations [40], the corresponding combined stress ratio is given by:

$$Sr^C = \left[\frac{M_u}{M_c} + \frac{P_u}{P_c}\right] + \left[\frac{V_u}{V_c} + \frac{T_u}{T_c}\right]^2 \leq 1 \tag{25}$$

3. THE OPTIMIZATION ALGORITHM

Recently, a number of nature-inspired optimization methods are introduced based on birds of prey behavior [28,42–44]. Among which, Falcon Optimization Algorithm (FOA) is concerned here that simulates hunting actions of falcons to catch their prey [28]. Falcon can adopt its hunting flight in three stages: i) seeking for the prey, ii) logarithmic-path flying to adjust the dive and iii) diving to catch the prey when close enough. At the first two stages, Falcon keeps an eye at the prey by looking sideways while in the third stage it uses binocular vision [45,46]. If the dive was not successful, Falcon may favor flaying back based on its cognitive experience. They can also compete each other as a common behavior in several birds of prey. Steps of the utilized FOA for the current structural optimization are as follows:

Step 1. Set the control parameters of the algorithm.

Step 2. At the first iteration, generate N_P randomly generated vectors based on uniform distribution as initial population of artificial birds. It is performed for every i^{th} individual by:

$$X_i = X_L + R \otimes (X_U - X_L) \tag{26}$$

where X_i is a D-dimensional vector between its lower and upper bounds of X_L and

[DOI: 10.22068/ijoce.2024.14.4.605]

X_U, respectively. The sign $\otimes$ stands for component-wise product while the function R is a D-dimensional vector of random numbers given as:

$$R = \{r_j | -1 \leq r_j \leq 1, j = 1,2,\dots,D\} \tag{27}$$

Initiate the limiting velocity vectors V^{min} and V^{max} by:

$$V^{max} = -V^{min} = \alpha(X^U - X^L) \tag{28}$$

The factor α is a positive control parameter lower than unity.

Step 3. Set the iteration number to $t = 1$. Decode every individual vector in the population to the corresponding structural model. Determine the constraints and their violation via structural analysis and calculate the structural weight. Then use them to evaluate fitness of each corresponding design vector. Initiate the global best position X^t_{gbest} as the fittest individual over the entire population.

Step 4. Increase the iteration number t by 1. Repeat the following main loop until the stopping criterion is satisfied:

- For the bird number i from 1 to N_P create a candidate individual X_i^{Cand} as:
  - If a random number with uniform distribution returned by the function r falls below AP, generate X_i^{Cand} by:

    $$X_i^{Cand} = X_i^{t-1} + V_i^{t-1} + rC_c\left(X_{i,pbest}^{t-1} - X_i^{t-1}\right) + rC_s\left(X_{gbest}^{t-1} - X_i^{t-1}\right) \tag{29}$$

    where $X_{i.pbest}^{t-1}$ denotes the best experience of each bird and X_{gbest}^{t-1} stands for the best position among of all of them. V_i^{t-1} gives the velocity of the ith bird. The cognitive and social factors are given by c_c and c_s, respectively.

  - otherwise
    - If the function r returns a value greater than DP, perform logarithmic flight as:

      $$X_i^{cand} = X_i^{t-1} + re^{br}\left(X_c - X_i^{t-1}\right) \tag{30}$$

      where X_c stands for a randomly picked bird over the population and b is a fixed control parameter.
    - Generate candidate solution X_i^{Cand} by flying toward X_c as a randomly chosen falcon in the population when X_c is fitter than the current falcon.

[DOI: 10.22068/ijoce.2024.14.4.605]

$$X_i^{Cand} = X_i^{t-1} + V_i^{t-1} + rf_c\left(X_c - X_i^{t-1}\right) \quad (31)$$

otherwise form X_i^{Cand} by a fly-back as:

$$X_i^{Cand} = X_i^{t-1} + V_i^{t-1} + rC_c\left(X_{i,pbest}^{t-1} - X_i^{t-1}\right) \quad (32)$$

Check for the velocity limit and fix the candidate solution by:

$$X_i^{cand} = X_i^{t-1} + \min\left(V^{max}, max\left(V^{mn}, X_i^{cand} - X_i^{t-1}\right)\right) \quad (33)$$

This way, the new velocity vector is forced to fall between $V^{\min}$ and $V^{\max}$

- Associate the design variables in X_i^{Cand} with their corresponding section indices and decode the candidate vector to the structural model.
- Analyze the structural model to evaluate fitness of the candidate vector.
- Greedy selection: Replace X_i^{t-1} with X_i^{Cand} if X_i^{Cand} is fitter than it.
- Update $X_{i,pbest}^{t}$

- Update X_{gbest}^{t}

Step 5. Announce X_{gbest}^{t} as the best solution obtained to the optimization problem.

Stopping criterion can be taken either $t = Iter_{\max}$ or $NFE = NFE_{\max}$. The iteration number is denoted by t while NFE stands for the number of objective function evaluations. In this study the former criterion is applied. Thus, the proposed optimization algorithm has $AP, DP, \alpha, b, c_c, c_s, f_c$ as its specific control parameters in addition to the common parameters of N_P and $Iter_{\max}$.

4. NUMERICAL INVESTIGATION

A number of diagrid models with various heights are considered for design optimization. Constructional material is Steel of the European grade St-37 with the yield stress of $235MPa$, elastic modulus of $200GPa$ and density of $7849kg/m^3$. Each model is subjected to simultaneous gravitational and lateral wind loading based on regulations of INBC [46].

[DOI: 10.22068/ijoce.2024.14.4.605]

Table 1: Loading combinations

Load Combination	Dead Load	Live Load	Wind load
1	1.4	0	0
2	1.2	1.6	0
3	1.2	0	0.7
4	1.2	1	1.4
5	0.9	0	1.4

Table 1 gives the code-based loading combinations applied in designing diagrids. Such models are assumed to be built on a region with the reference wind velocity of $130\,km/h$. INBC regulations exert wind load as pressure on windward, leeward and other sides of the building after generating the height-wise pressure profile from the base-wind-pressure. The height-wise distribution of windward pressure is given by INBC as:

$$P_{(z)} = P_0 I_w C_e C_g C_P \tag{34}$$

The base-wind-pressure is denoted by P_0. The factors $I_w C_e C_g C_P$ are calculated due to the INBC design code to distribute p_0 among the height and different sides of the building structure. Figure 1 demonstrates schematic wind loading on a three-dimensional model due to INBC procedure.

In the present work, gravitational and wind loadings are spatially exerted on three-dimensional symmetric models; however, they are then reduced into equivalent planar models to allow faster analysis and convergence during optimal design due to high cardinality of the search space. Diagrid examples are considered with three different number of stories as depicted in Figure 2.

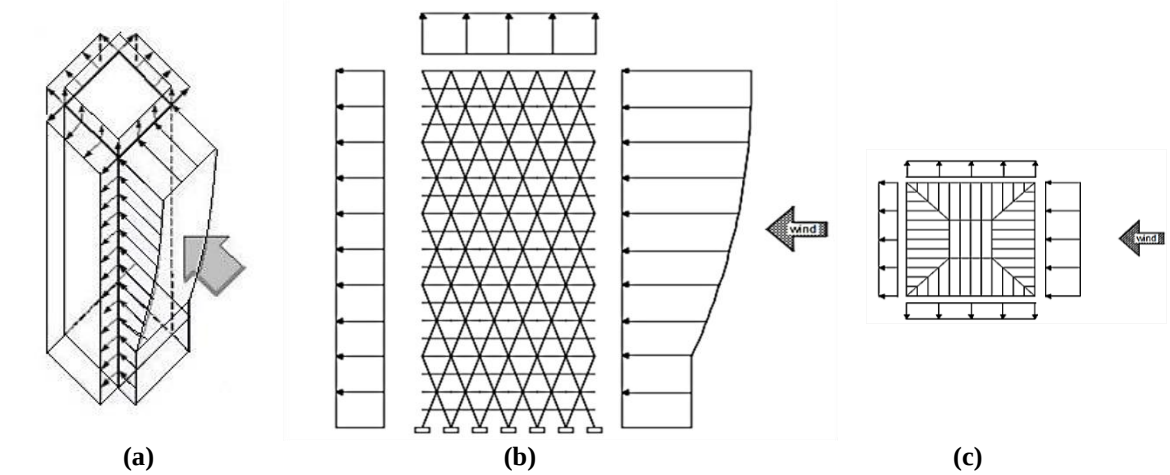

Figure 1: Typical wind loading profile: (a) 3D view, (b) side view and (c) plan view

[DOI: 10.22068/ijoce.2024.14.4.605]

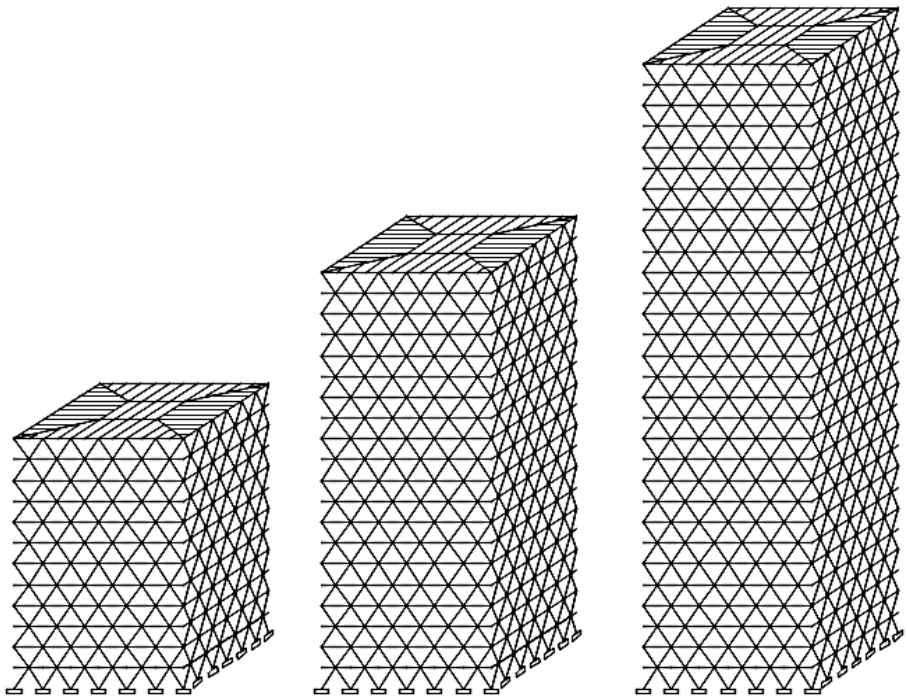

Figure 2: Variation of diagrid height (number of stories) in the treated examples

Geometry of a diagrid model may vary with variation of diagonal angles with respect to the horizon. It is worthy to notify that such angles cannot take all continuous values for a prescribed story height and bay length. Instead, they can be associated with some discrete values by varying the number of stories and/or bays that are covered in the diagrid module. A regular diagrid is distinguished with uniform angle and topological density of diagonal members among the structure. For example, a 20-story regular diagrid can be subdivided into 5 four-story panels, each one covered by a single diagonal unit among its height. Alternatively, it can also be subdivided into 20 one-story panels or 10 two-story panels. For the story-height of 3*m* and the bay-length of 4*m*, there are three alternative angles: $56.3°$, $71.6°$ and $80.5°$. Figure 3 illustrates three possible configurations for 20-story diagrids with identical plan. The effect of soil flexibility on the optimal design is also modeled by inserting vertical springs beneath the foundations.

In the present study, the planar diagrid models are named by the general notation of. $nJ\theta$ For each specific model, n is replaced with the corresponding number of stories, θ denotes the diagrid angle with the horizontal line and J is replaced with r for the rigid-base models or with f for the case of flexible-base. For example, 20f71 stands for the 20-story model on the flexible-soil having the uniform diagrid angle of $71.6°$.

[DOI: 10.22068/ijoce.2024.14.4.605]

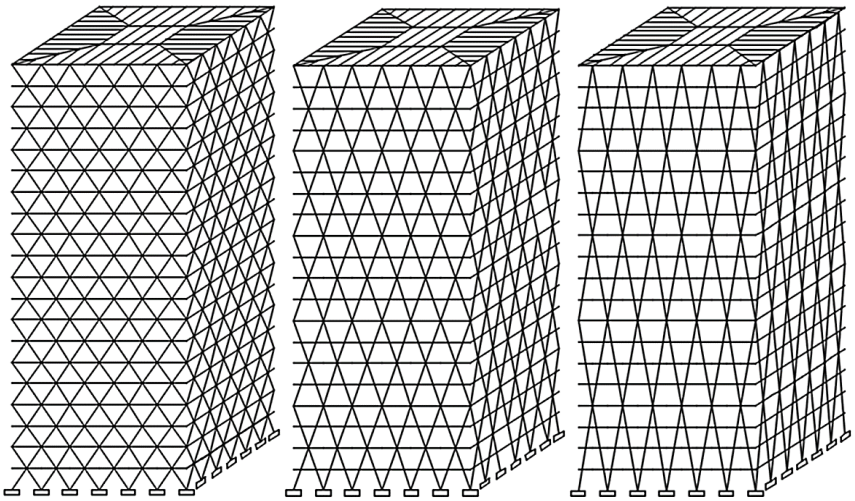

(a) **(b)** **(c)**

Figure 3: Variation of diagrid angle in the 20-story example: (a) 56.3o, (b) 71.6 o and (c) 80.5o

For any diagrid angle, the optimization is started from identical population to preserve true comparison between the rigid-base and the flexible-base cases. The control parameters of the algorithm are applied in accordance with Table 2. Notation of the diagrid models with various diagonal angles and boundary conditions are given in Table 3 together with the search space cardinality of each case. It can be noticed that such models constitute discrete optimization problems with the search space sizes in the orders of 10^8 to 10^{57} .

Table 2: Applied control parameters of the proposed FOAs

Common parameters		Specific parameters						
N_P	$Iter_{\max}$	AP	DP	α	b	c_c	c_s	f_c
15	300	0.1	0.8	0.1	1.0	2.0	2.0	2.0

Table 3: General characteristics of the treated diagrid models

Model ID	Number of stories	Boundary condition at base	Diagrid angle	D	Search Space Cardinality
12r56	12	Rigid	56.3°	15	$28^{15} \sim 5.1\times10^{21}$
12f56	12	Flexible	56.3°	15	$28^{15} \sim 5.1\times10^{21}$
12r71	12	Rigid	71.6°	9	$28^{9} \sim 1.0\times10^{13}$
12f71	12	Flexible	71.6°	9	$28^{9} \sim 1.0\times10^{13}$
12r80	12	Rigid	80.5°	6	$28^{6} \sim 4.8\times10^{8}$
12f80	12	Flexible	80.5°	6	$28^{6} \sim 4.8\times10^{8}$
20r56	20	Rigid	56.3°	24	$28^{24} \sim 5.4\times10^{34}$
20f56	20	Flexible	56.3°	24	$28^{24} \sim 5.4\times10^{34}$
20r71	20	Rigid	71.6°	15	$28^{15} \sim 5.1\times10^{21}$
20f71	20	Flexible	71.6°	15	$28^{15} \sim 5.1\times10^{21}$
20r80	20	Rigid	80.5°	10	$28^{10} \sim 2.9\times10^{14}$
20f80	20	Flexible	80.5°	10	$28^{10} \sim 2.9\times10^{14}$

[DOI: 10.22068/ijoce.2024.14.4.605]

30r56	30	Rigid	56.3°	36	$40^{36} \sim 4.7\times10^{57}$
30f56	30	Flexible	56.3°	36	$40^{36} \sim 4.7\times10^{57}$
30r71	30	Rigid	71.6°	23	$40^{23} \sim 7.0\times10^{36}$
30f71	30	Flexible	71.6°	23	$40^{23} \sim 7.0\times10^{36}$
30r80	30	Rigid	80.5°	16	$40^{16} \sim 4.3\times10^{25}$
30f80	30	Flexible	80.5°	16	$40^{16} \sim 4.3\times10^{25}$

For the sake of conciseness, one case of flexible soil is considered against the rigid-base boundary condition. Applying three height alternatives (12, 20 and 30 stories), three possible angles for the regular diagrids and two cases of boundary conditions; a total of 18 distinct models are studied. Note that since FOA is a stochastic algorithm, it is required to perform several independent runs (at least 10) for every distinct model to take sufficiently reliable statistical results. According to Table 2, every optimization run in our study needs at least 4500 structural analyses. The mater makes sense about how computationally expensive is such a task and why static analyses are used for the optimal design. For such a design procedure the code of practice [44] offers to consider the effect of turbulences on taller examples by applying proper values of C_g.

According to INBC as the design code, soil types are distinguished in 4 groups. The soil type IV is too loose to withstand loadings in high-rise buildings. Therefore, the soil type III is considered in the current study; for which the shear wave velocity $\bar{V}_s$ varies between $175\,m/s$ to $375\,m/s$ [47]. Here the mean value in such a range is considered to derive the soil shear modulus by the following well-known relation:

$$G = \frac{\gamma_s}{g}\bar{V}_s^2 \tag{35}$$

Where $\bar{V}_s$ stands for the mean shear wave velocity in top 30 meters of the soil with the density of γ_s and $g = 9.807\ N/kg$ denotes the gravitational constant. The stiffness of the equivalent spring for such a soil type is derived based on the soil shear modulus G and Poisson ratio ν. It is given by [48] for a square foundation with the width B in the vertical and horizontal directions as:

$$K_z = 4.54GB\frac{\nu}{1-\nu} \tag{36}$$

$$K_x = 9.00GB\frac{1}{2-\nu} \tag{37}$$

Assuming $\bar{V}_s = 275\,m/s$ in average for a soil type III with the density of $1800\,kg/m^3$, leads to $K_z = 1795MN/m$ as the vertical stiffness of the equivalent springs while $K_x = 2.72K_z$ for a Poisson ratio of 0.3. Every such spring is joined with the base node in the corresponding diagrid model. Stiffness matrix of a linear spring with two nodes, is implemented in the following form:

[DOI: 10.22068/ijoce.2024.14.4.605]

$$k_e = \begin{bmatrix} k_s & -k_s \\ -k_s & k_s \end{bmatrix} \tag{38}$$

Once the second node of such a spring is attached to a *Degree Of Freedom* (DOF) at the structure's base, the second diagonal of the above matrix is assembled to that DOF in the total stiffness matrix. The stiffness coefficient k_s in the matrix K_e can represent k_x or k_z for a horizontal or a vertical soil spring, respectively.

4.1 The 12-Story Example

This example is designed with diagrid angles of $56.3°$, $71.6°$ and $80.5°$ using the discrete list of structural sections given in Table 4**.** For each angle two boundary conditions are also applied; i.e. the rigid and the flexible foundation models. Configuration and member grouping of the models are demonstrated in Figures 4 and 5. It can be noted that switching the boundary condition does not alter the member grouping. The first model is characterized with 15 member groups while the second and the third include 9 and 6 groups, respectively. Noting that such member groups correspond the design variables to be associated with the section indices of Table 4, the search space cardinality will be of different orders from 10^{21} in the $56.3°$ models to 10^{8} in the $80.5°$ ones.

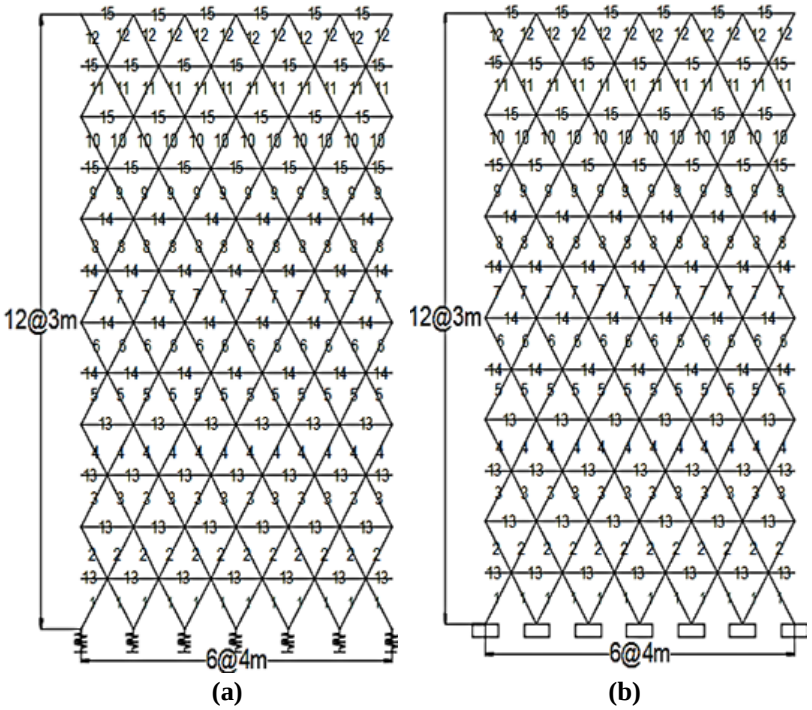

(a) **(b)**

Figure 4: Configuration and member grouping of the diagrid models: (a) 12f56 and (b) 12r56

Table 5 compares the section indices and optimal weight results between 12r56 and 12f56 models. It is noted that for the diagrid angle of $56.3°$, the optimal design on flexible soil has heavier weight than with the rigid boundary condition. The best weight for 12r56

[DOI: 10.22068/ijoce.2024.14.4.605]

and 12f56 models are nearly 36.0 ton and 45.9 ton, respectively. A similar trend is observed in the corresponding mean results of 40390.30 kg and 41975.18 kg, respectively.

Table 4: List of available sections for the 12-story and 20-story diagrid models

Section ID	Section Name	Area ($10^{-4}m^2$)	Section ID	Section Name	Area ($10^{-4}m^2$)
1	W10x19	36.26	15	W12x72	136.13
2	W10x33	62.65	16	W12x79	149.68
3	W10x39	74.19	17	W12x87	165.16
4	W10x49	92.90	18	W12x96	181.94
5	W10x54	101.94	19	W14x22	41.87
6	W10x60	113.55	20	W14x43	81.29
7	W10x77	145.8	21	W6x15	28.58
8	W12x19	35.94	22	W6x20	37.87
9	W12x26	49.35	23	W8x24	45.68
10	W12x30	56.71	24	W8x28	53.23
11	W12x45	85.16	25	W8x31	58.90
12	W12x53	100.64	26	W8x35	66.45
13	W12x58	109.68	27	BOX 400X20mm	304.00
14	W12x65	123.23	28	BOX 550X25mm	525.00

Table 5: Optimization results for 12r56 and 12f56 models

Group number	Diagrid Model	
	12r56	12f56
1	19	11
2	23	11
3	8	9
4	10	9
5	21	10
6	8	8
7	22	24
8	3	12
9	25	23
10	8	8
11	6	8
12	9	23
13	19	14
14	8	10
15	14	14
Best weight (kg)	36017.52	45895.33
Mean weight (kg)	40390.30	41975.18
C.V.	0.06	0.07

Table 6: Optimization results for 12r71 and 12f71 models

Group number	Diagrid Model	
	12r71	12f71
1	21	8
2	21	22
3	8	1
4	9	10
5	23	21

[DOI: 10.22068/ijoce.2024.14.4.605]

6	19	21
7	21	10
8	13	9
9	12	12
Best weight (kg)	31851.99	28896.70
Mean weight (kg)	32078.99	31436.72
C.V.	0.06	0.06

Table 6 shows a different trend for the diagrid angle of $71.6°$. In this case, the 12f71 model has led to smaller weight than the corresponding rigid-base model; both in the best and mean results. The best designs for the 12r71 and 12f71 models weigh almost 31.9 ton and 28.9 ton, respectively.

For the angle of $80.5°$, the results are briefed in Table 7. It can be noticed that the best weight is obtained 41.7 ton for the rigid-base that is slightly lower than 45.7 ton for the flexible-base; however, the corresponding mean results exhibit a reverse order.

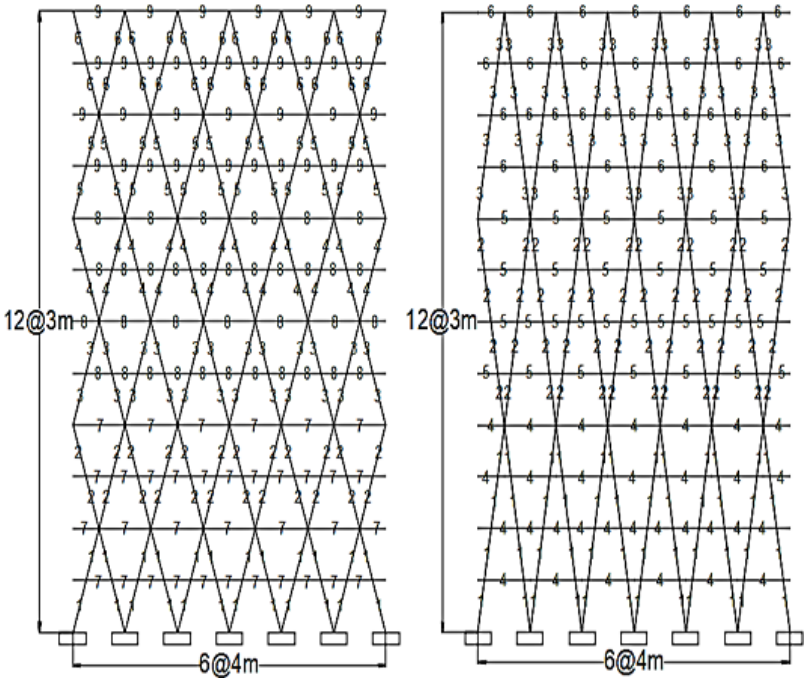

(a) **(b)**

Figure 5: Configuration and member grouping of the diagrid models: (a) 12r71 and (b) 12r80

Figure 6 compares convergence traces of the 12-story diagrid models; denoting the flexible cases with dashed lines. The first rank over the rigid-base models, belongs to 12r71 weighing 31852 kg while 12r56 and 12r80 stand on the 2nd and 3rd ranks, respectively. Furthermore, it is found that the 12f71 can withstand the loading combinations with the lowest weight of 28896.70 kg among all the others. It is 20% and 31% lighter than the best optimal weight in the $56.3°$ and $80.5°$ cases, respectively.

[DOI: 10.22068/ijoce.2024.14.4.605]

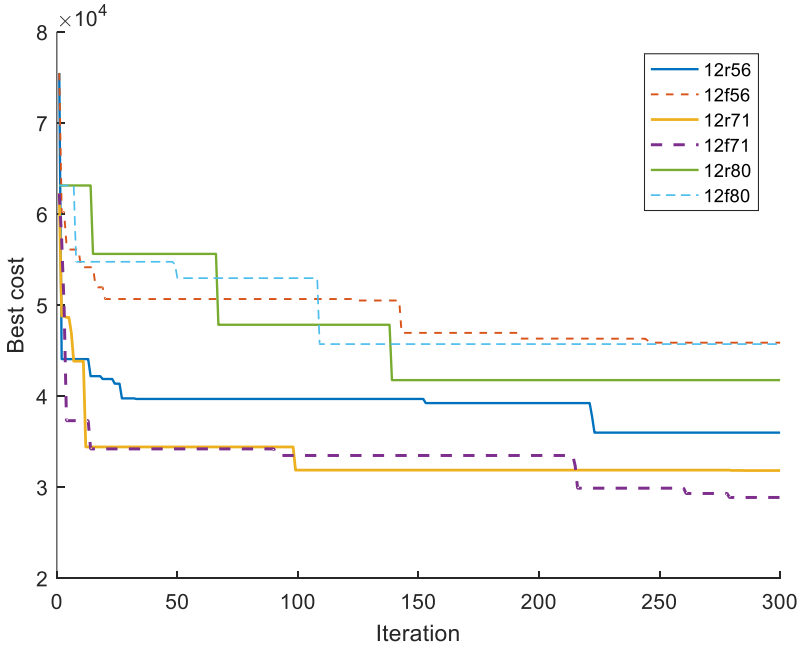

Figure 6: Convergence curves for optimization of the 12-story diagrid models

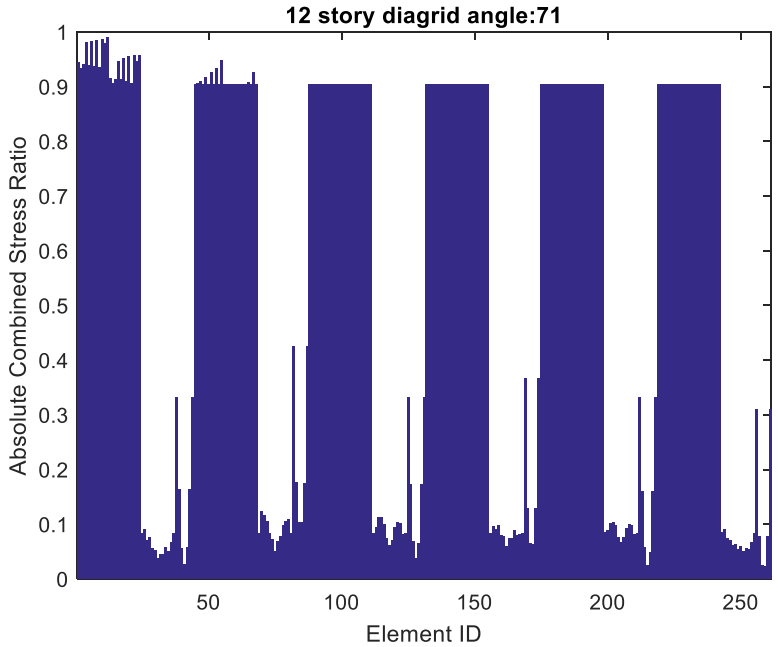

Figure 7: Constraint satisfaction in the best design of 12-story diagrid

Figure 7 confirms how such a design has satisfied the stress constraint over the structural elements under the load combinations of Table 1. It can be noticed that the highest stress ratio has approached the allowable limit of 1 in the feasible 12r71 model with the cardinality

[DOI: 10.22068/ijoce.2024.14.4.605]

of 10^{13}. Due to the proposed formulation of the optimization problem, activating such a behavior constraint can declare optimal use of the construction material; however, the side constraints are preserved by selecting form the available list of sections.

Table 7: Optimization results for 12r80 and 12f80 models

Group number	Diagrid model	
	12r80	12f80
1	21	8
2	22	19
3	8	25
4	8	1
5	25	25
6	27	27
Best weight (kg)	41785.08	45741.73
Mean weight (kg)	50886.74	43599.64
C.V.	0.45	0.18

4.2 The 20-Story Example

This example is modeled with three different diagrid angles of Figure 3; each one studied via two boundary conditions. The corresponding member groupings are given by Figures 8 and 9. Twenty-eight available sections of Table 4 are employed for sizing optimization of the 20-story models.

According to Table 3, cardinality of the search space in the $56.3°$ case is 5.4×10^{34}; i.e. about 10^{13} times larger than the corresponding case in the previous example. The lowest cardinality among $56.3°$, 71.6^{o} and $80.5°$ cases, belongs to the latter one; that is of the order 10^{14}.

According to Figure 10, in $56.3°$ and $80.5°$ cases, the rigid-base boundary condition has led to lighter weight than the flexible-base. Tables 8 and 9 confirm such a trend for the mean results; however, it is not the case in Table 10.

Figure 10 also reveal that the best optimal weight among 20-story models belongs to 20f71. According to Figure 10, the final stages of convergence curves for the rigid-base cases have fallen below the flexible-cases except the flexible-case of 12f71 model. Table 9 reveals the least weight of 52083.13 kg for 20f71 that is 20% lighter than 20r71.

[DOI: 10.22068/ijoce.2024.14.4.605]

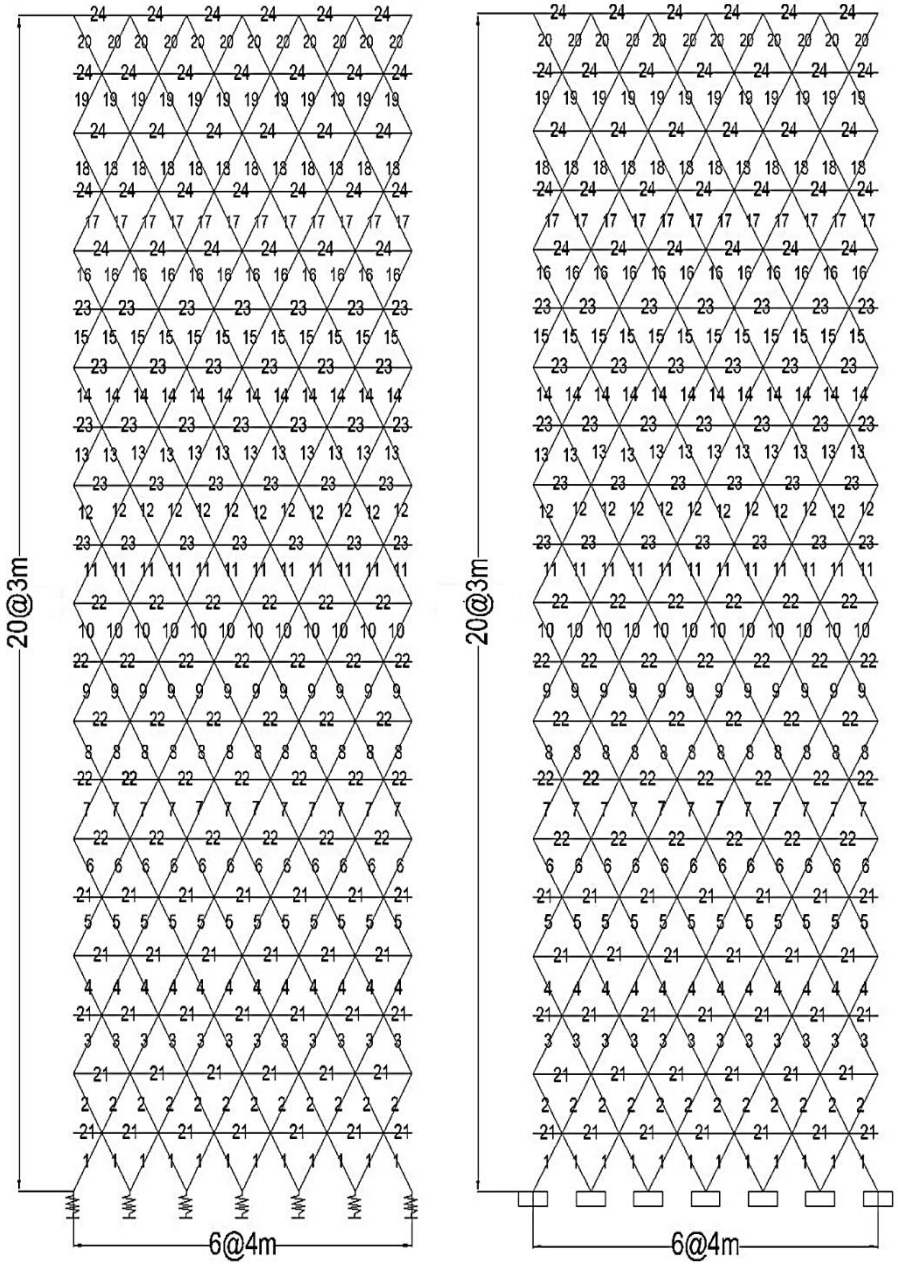

(a) **(b)**

Figure 8: Configuration and member grouping of the diagrid models: (a) 20f56 and (b) 20r56

Such an optimal weight is also more than 30% lighter than the best results of $56.3°$ and $80.5°$ cases. It can be observed in Figure 11 that 20f71 design has successfully satisfied the stress constraint. Furthermore, activation of such a behavior constraint confirms that 20-

[DOI: 10.22068/ijoce.2024.14.4.605]

story diagrid with the angle of 71.6^{o} at flexible soil has optimally used the material strength to withstand the loading combinations of Table 1.

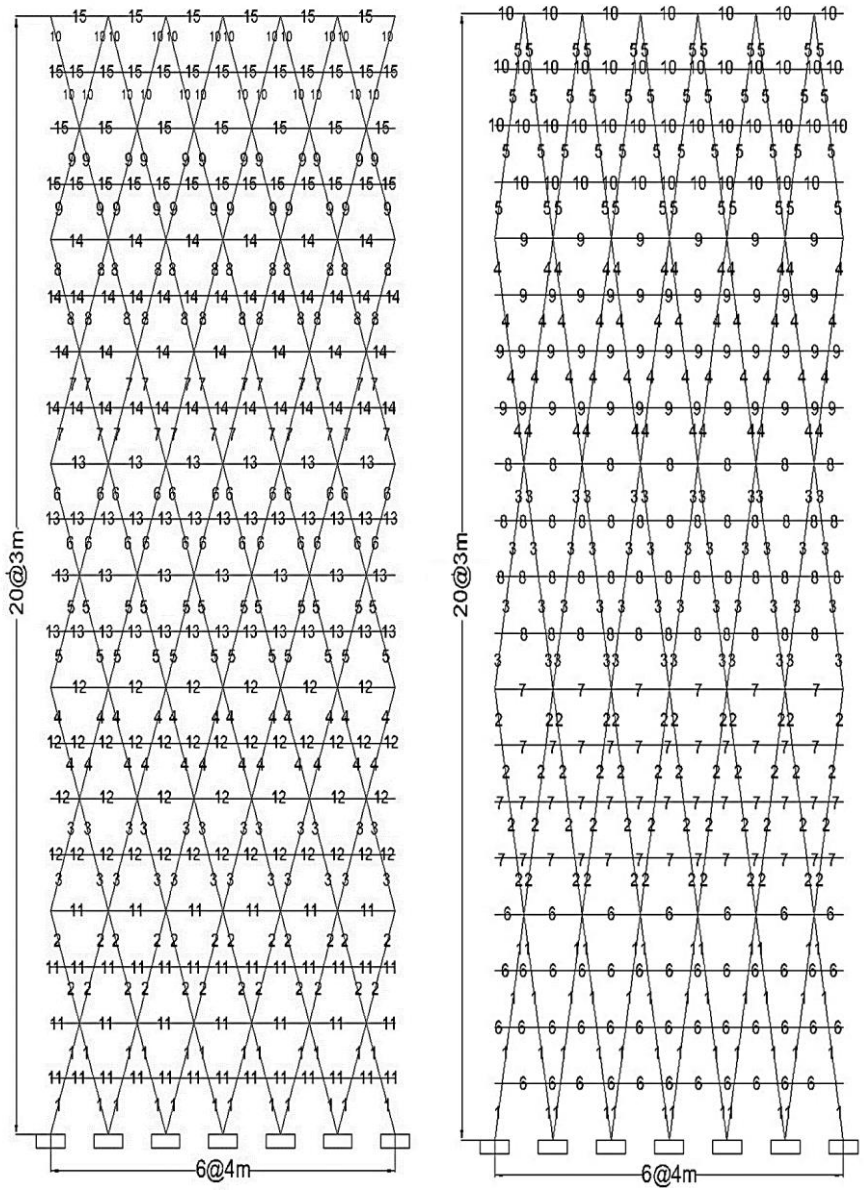

(a) **(b)**

Figure 9: Configuration and member grouping of the diagrid models: (a) 20f71 and (b) 20r80

4.3 The 30-Story Example

Here, a taller example with 30-stories is studied. The spatial diagrids have been reduced to their planar equivalent models as depicted in Figures 12 and 13. For such a large-scale example some heavier sections are needed to withstand the applied loadings. Therefore, a

[DOI: 10.22068/ijoce.2024.14.4.605]

larger set with respect to previous examples is applied within 40 sections of Table 11. The models are distinctly optimized in three cases of diagrid angles; i.e. $56.3°$, $71.6°$ and $80.5°$ applying the flexible and rigid-base boundary conditions. Due to the number of member groups and available sections, the corresponding search space cardinalities are reported in Table 3 that are considerably higher than previous examples.

Figure 14 shows convergence curves of the best designs for each case of this examples. It can be realized that 30r56 has ended with the heaviest design while the final weights of 30r71and 30r80 have fallen between the least weight by 30f71 and the results of the other cases. Further information can be derived from Tables 12-14. For the $56.3°$ case, Table 12 reveals that despite some previous examples, 30f56 has led to less weights than 30r56 both in the best and mean results. Table 14 reports similar trend in the mean results of the $80.5°$ case. However, the best results of this case do not obey such a trend.

Table 8: Optimization results for 20r56 and 20f56 models

Group number	Diagrid model	
	20r56	20f56
1	8	1
2	8	8
3	11	8
4	12	23
5	9	23
6	11	26
7	21	23
8	7	1
9	21	5
10	21	13
11	19	26
12	16	23
13	9	8
14	21	21
15	25	22
16	8	21
17	1	1
18	19	5
19	6	8
20	24	17
21	16	18
22	22	9
23	21	11
24	18	18
Best weight (kg)	79365.04	85721.58
Mean weight (kg)	90100.81	91167.51
C.V.	0.08	0.06

[DOI: 10.22068/ijoce.2024.14.4.605]

According to Table 13, the optimal design of 30f71 has led to the least weight of 99199.61 kg that is 12% lighter than the best result of 30r71. Meanwhile, the mean results of 30r71 and 30f71 show just a 4% difference.

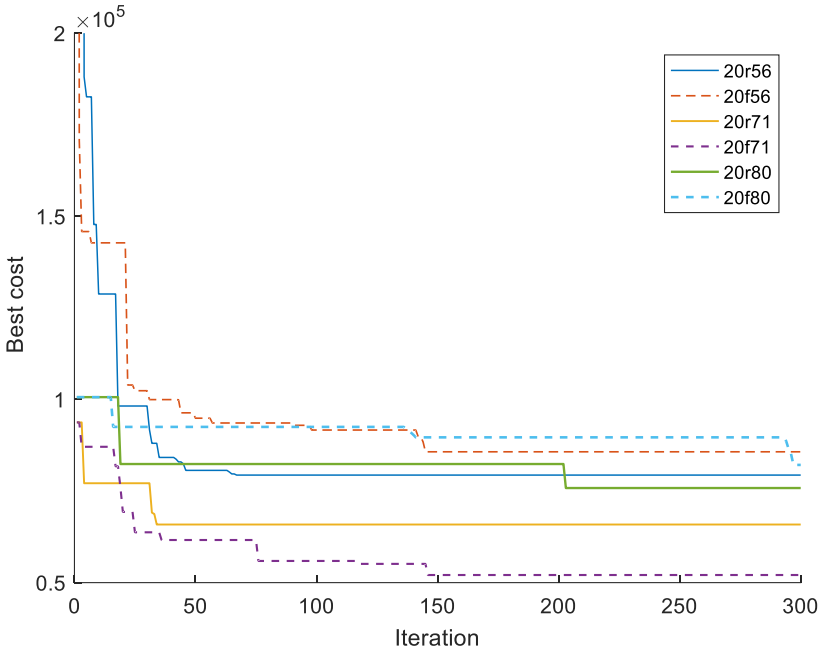

Figure 10: Convergence curves for optimization of the 20-story diagrid models

Table 9: Optimization results for 20r71 and 20f71 models

Group number	Diagrid model	
	20r71	20f71
1	23	9
2	25	9
3	1	9
4	1	1
5	26	8
6	6	8
7	1	21
8	26	20
9	1	10
10	24	8
11	10	9
12	10	23
13	5	22
14	3	23
15	16	16
Best weight (kg)	65868.56	52083.13
Mean weight (kg)	62827.52	64763.77
C.V.	0.06	0.10

[DOI: 10.22068/ijoce.2024.14.4.605]

Table 10: Optimization results for 20r80 and 20f80 models

Group number	Diagrid model	
	20r80	20f80
1	23	13
2	21	19
3	8	1
4	21	9
5	19	21
6	21	22
7	20	10
8	22	21
9	25	22
10	28	28
Best weight (kg)	75829.08	82142.36
Mean weight (kg)	140713.50	104619.60
C.V.	0.62	0.47

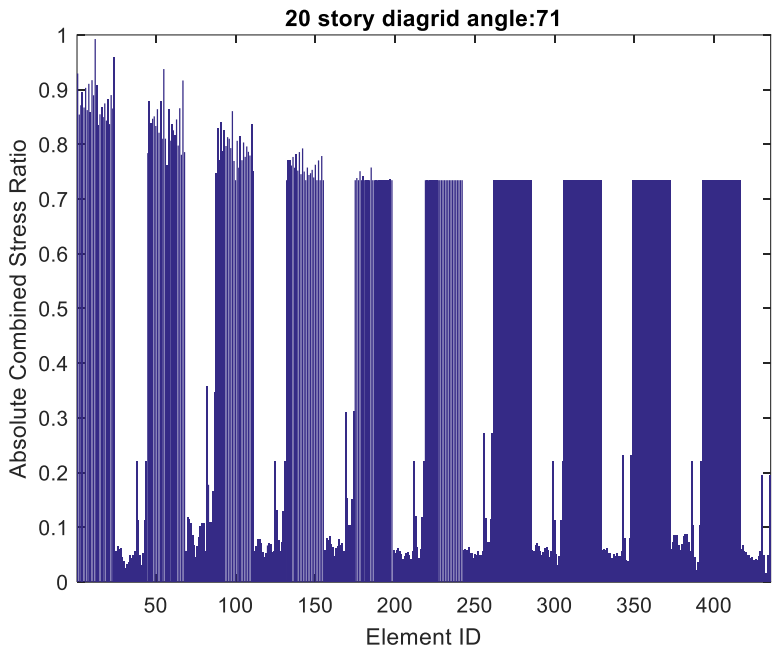

Figure 11: Constraint satisfaction in the best design of 20-story diagrid

5. DISPLACEMENT AND DRIFT RESPONSES

One of the common issues in design of high-rise buildings is to confine story sways against lateral loading. Although diagrid has already been reported as an efficient structural system to withstand lateral loads [1], such an issue is further studied in the present study, after weight minimization of the diagrid models.

[DOI: 10.22068/ijoce.2024.14.4.605]

Table 11: List of available sections for the 30-story diagrid models

Section ID	Section Name	Area ($10^{-4}m^2$)	Section ID	Section Name	Area ($10^{-4}m^2$)
1	W10X19	36.26	21	W8X24	45.68
2	W10X33	62.65	22	W8X28	53.23
3	W10X39	74.19	23	W8X31	58.90
4	W10X49	92.9	24	W8X35	66.45
5	W10X54	101.94	25	W8X40	75.48
6	W10X60	113.55	26	W8X48	90.97
7	W10X77	145.81	27	W12X120	227.74
8	W12X19	35.94	28	W12X136	257.42
9	W12X26	49.35	29	W12X152	288.39
10	W12X30	56.71	30	W12X170	322.58
11	W12X45	85.16	31	HSS14X14X5/16	101.29
12	W12X53	100.64	32	HSS16X16X5/16	116.77
13	W12X58	109.68	33	HSS16X16X5/8	225.81
14	W12X65	123.23	34	BOX 300X20mm	224.00
15	W12X72	136.13	35	BOX 400X20mm	304.00
16	W12X79	149.68	36	BOX 500X25mm	475.00
17	W12X87	165.16	37	BOX 550X25mm	525.00
18	W12X96	181.94	38	BOX 600X25mm	575.00
19	W14X22	41.87	39	BOX 700X25mm	675.00
20	W14X43	81.29	40	BOX 700X30mm	804.00

Figure 16 illustrates profiles of lateral displacement vs. the structural height (the story number). It is evident that all the models have a general trend of sway increase with height; in agreement with cantilever truss-like behavior of such lateral-resisting systems. However, the range of maximum displacements increases for the taller diagrid systems. It can also be noticed that the configurations of $80.5°$ show more difference with the other two angles and critically highlights the difference between flexible and fixed-base cases. The difference between $56.3°$ and $71.6°$ configurations is more for lower-rise 12-story model. Furthermore, sway trend of $71.6°$ geometry has approached the $56.3°$ case in the taller models with 20 and 30 stories; indicating superiority of such configuration. Table 15 better declares how story-displacements increase with the structural height for every distinct case of diagrid geometry. It can be derived that the ratio of maximum lateral displacement over the total structural height, is confined to 0.003, 0.006 and 0.010 in the 12, 20 and 30 story examples, respectively.

Figure 17 reveals the differences between the considered models from another point of view; that is variation of inter-story drifts with the floor level. The $80.5°$ configuration, exhibits severer fluctuations in drift profile with respect to the other diagrid geometries. More uniform variation of inter-story drift with height can be found in the flexible-based models. Similar to lateral displacements; such drift values are in greater range for taller examples.

It can be realized that the drift ratio falls below one percent of the story height in most cases except 30f80 (and slightly in 30f56 and 30r80). According to Figure 19, the diagrid angle of $80.5°$ constitutes the most critical cases of lateral displacements. In this regard,

[DOI: 10.22068/ijoce.2024.14.4.605]

$71.6°$ has been the best angle in 20- and 30-story examples, while the first rank in 12-story models belongs to the diagrid angle of $56.3°$.

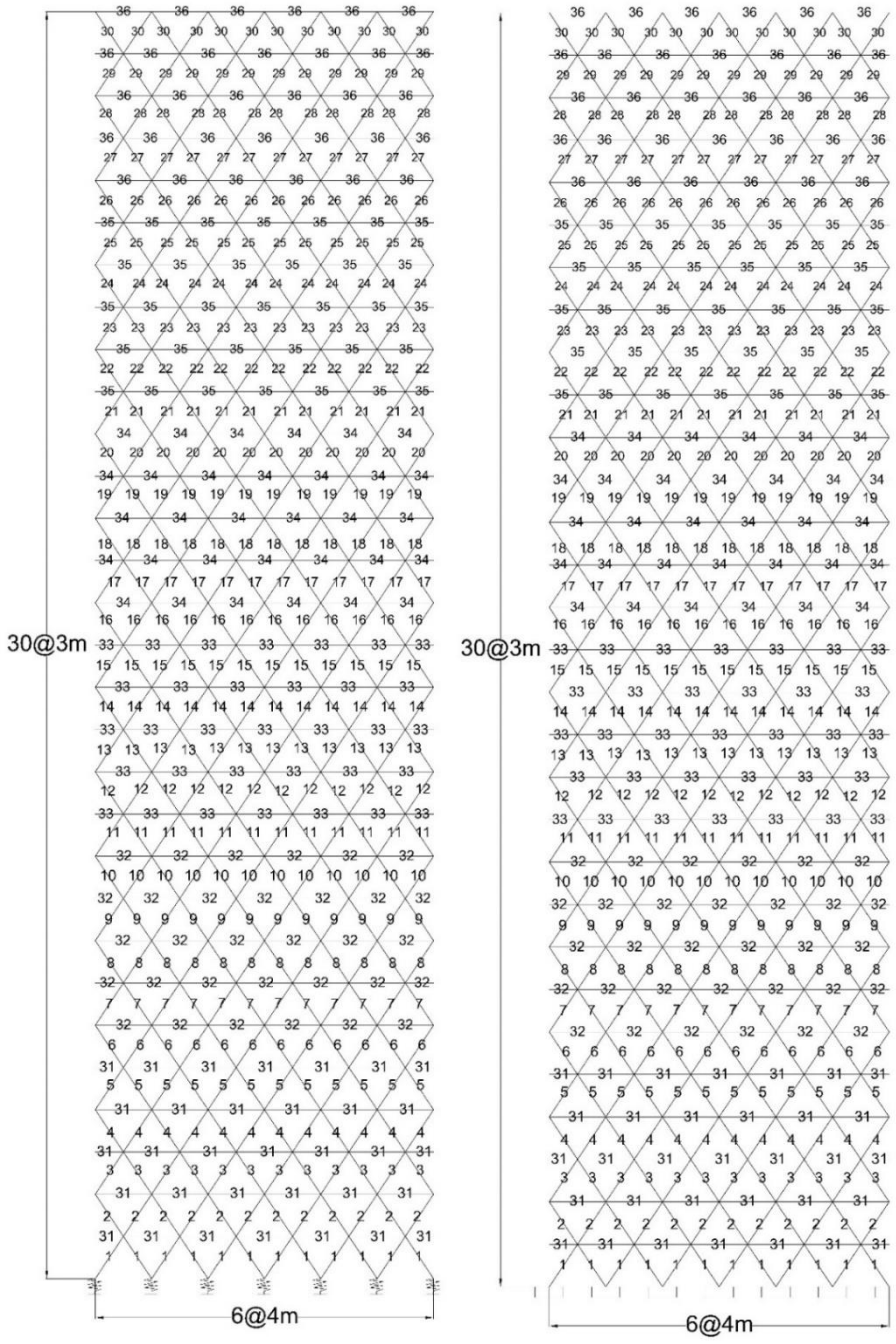

(a) **(b)**

Figure 12: Configuration and member grouping of the diagrid models (a) 30f56 and (b) 30r56

[DOI: 10.22068/ijoce.2024.14.4.605]

Table 12: Optimization results for 30r56 and 30f56 models

Group number	Diagrid model	
	30r56	30f56
1	27	25
2	22	23
3	21	19
4	26	25
5	26	26
6	20	21
7	26	22
8	23	22
9	11	8
10	8	10
11	20	15
12	6	9
13	19	21
14	10	10
15	20	21
16	21	22
17	21	25
18	19	20
19	11	17
20	26	24
21	18	20
22	21	20
23	26	26
24	22	13
25	25	23
26	14	11
27	20	27
28	26	25
29	23	25
30	23	23
31	21	21
32	19	19
33	22	21
34	21	23
35	20	22
36	36	36
Best weight (kg)	151649.20	146213.30
Mean weight (kg)	185062.70	182191.40
C.V.	0.14	0.14

[DOI: 10.22068/ijoce.2024.14.4.605]

[DOI: 10.22068/ijoce.2024.14.4.605]

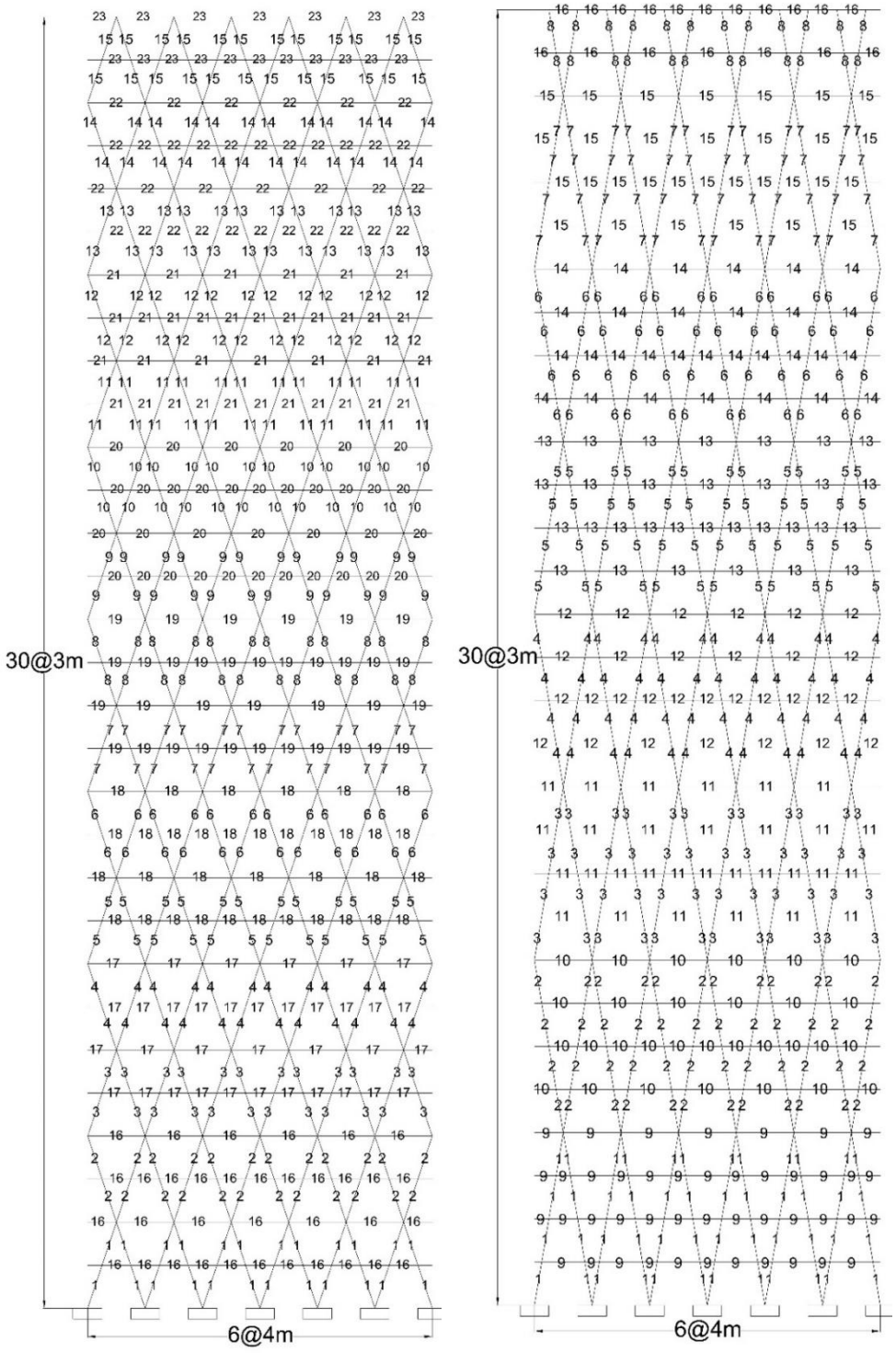

(a) **(b)**

Figure 13: Configuration and member grouping of the diagrid models (a) 30r71 and (b) 30r80

Table 13: Optimization results for 30r71 and 30f71 models

Group number	Diagrid model	
	30r71	30f71
1	11	26
2	9	21
3	25	21
4	17	22
5	24	23
6	25	25
7	21	22
8	16	23
9	25	19
10	21	21
11	21	21
12	19	22
13	1	13
14	21	20
15	9	9
16	15	14
17	1	23
18	32	22
19	8	10
20	5	22
21	21	24
22	9	19
23	35	29
Best weight (kg)	113165.1	99199.61
Mean weight (kg)	122725.1	127888.1
C.V.	0.08	0.17

The drift values are summarized in Table 16; exhibiting similar trend. The greatest drifts in different heights; i.e. 1.5, 2.9 and 4.8cm belong to the 12r80, 20f80 and 30f80 models, respectively. It indicates that the angle of $80.5°$ has been the worst case in decreasing the inter-story drifts. In the other hand, the least drifts in 20- and 30-story models belong to the $71.6°$ configuration on fixed-base by 0.21 cm and 0.99 cm; i.e. 34% and 48% of the corresponding largest values, respectively. Such a ratio is at most 14% among the 12-story models that indicates higher effect of geometry in the lower-rise example. Maximum drift values are graphically compared in Figure 18. It can be realized that drift ratio falls below one percent.

Table 14: Optimization results for 30r80 and 30f80 models

Group number	Diagrid model	
	30r80	30f80
1	19	19
2	24	19
3	13	22

[DOI: 10.22068/ijoce.2024.14.4.605]

4	22	23
5	21	26
6	8	20
7	23	12
8	23	31
9	23	31
10	1	10
11	22	23
12	19	24
13	19	23
14	10	15
15	10	15
16	40	40
Best weight (kg)	106882.9	136111.4
Mean weight (kg)	164829.9	155718.5
C.V.	0.41	0.33

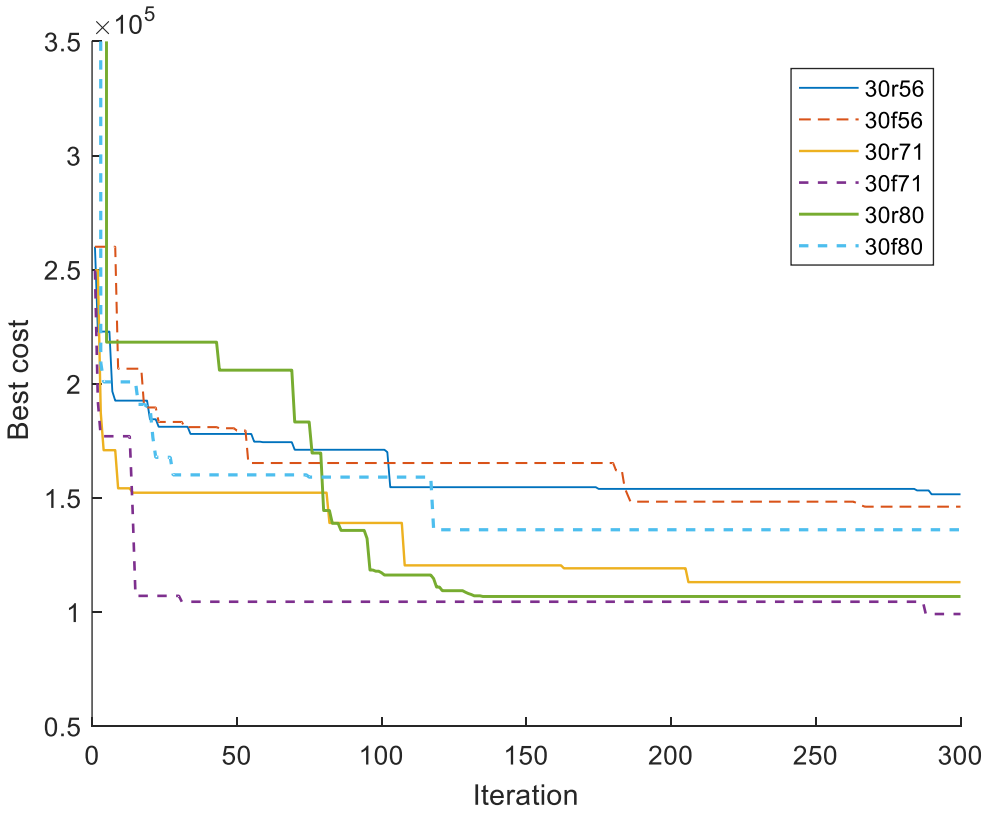

Figure 14: Convergence curves for optimization of the 30-story diagrid models

[DOI: 10.22068/ijoce.2024.14.4.605]

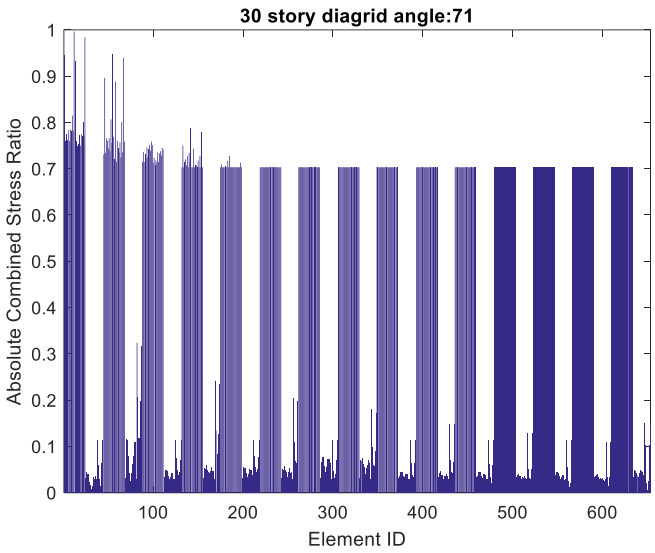

Figure 15: Constraint satisfaction in the best design of 30-story diagrid

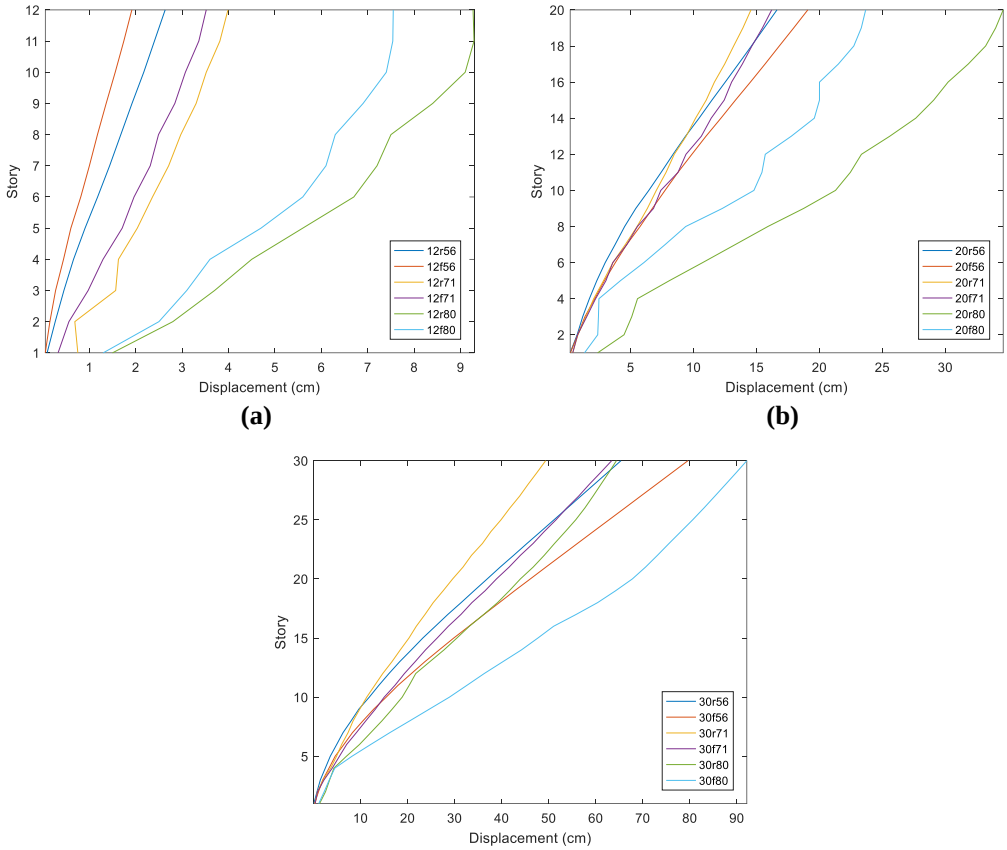

Figure 16: Variation of lateral displacement in (a) 12-story, (b) 20-story and (c) 30-story models

[DOI: 10.22068/ijoce.2024.14.4.605]

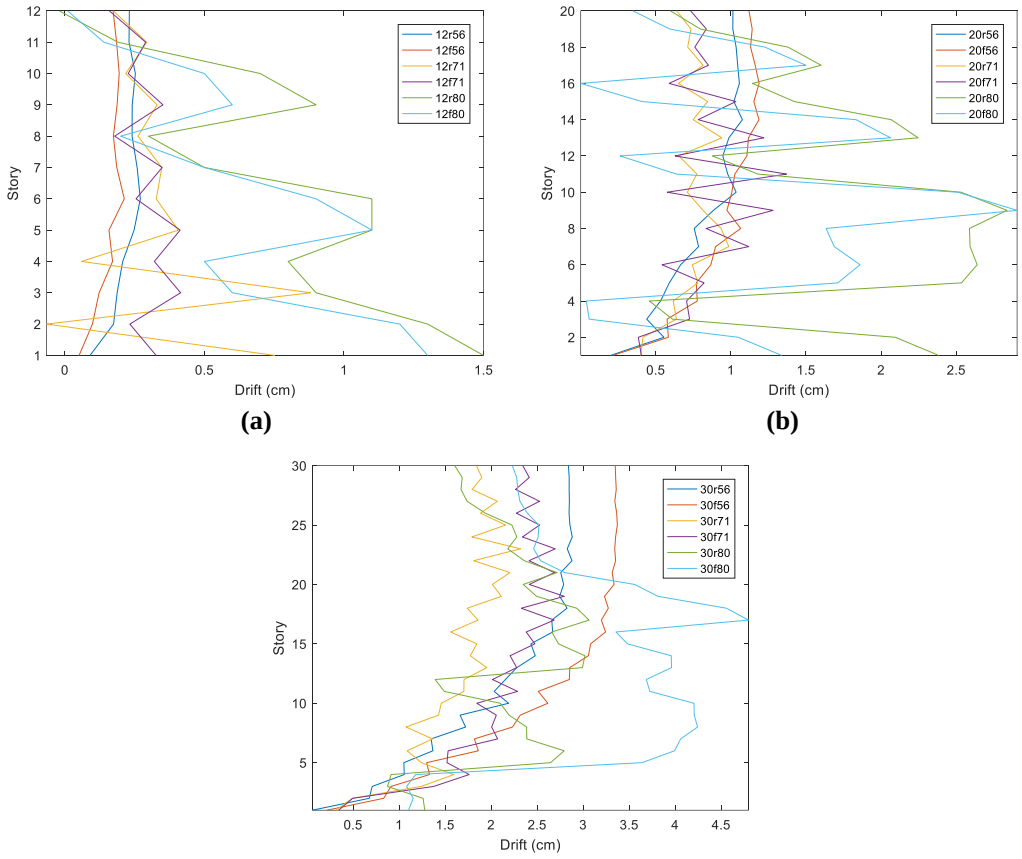

Figure 17: Variation of inter-story drift in (a) 12-story, (b) 20-story and (c) 30-story models

Table 15: Maximum lateral displacements (cm) in the diagrid models

(n)	(n)r56	(n)f56	(n)r71	(n)f71	(n)r80	(n)f80
12	2.6	1.9	4.0	3.5	9.3	7.6
20	16.6	19.1	14.6	16.2	34.6	23.7
30	65.4	79.6	49.3	63.4	64.4	92.1

Table 16: Maximum inter-story drift (cm) in the diagrid models

(n)	(n)r56	(n)f56	(n)r71	(n)f71	(n)r80	(n)f80
12	0.3	0.2	0.9	0.4	1.5	1.3
20	1.0	1.2	1.0	1.4	2.8	2.9
30	2.9	3.4	2.3	2.8	3.1	4.8

[DOI: 10.22068/ijoce.2024.14.4.605]

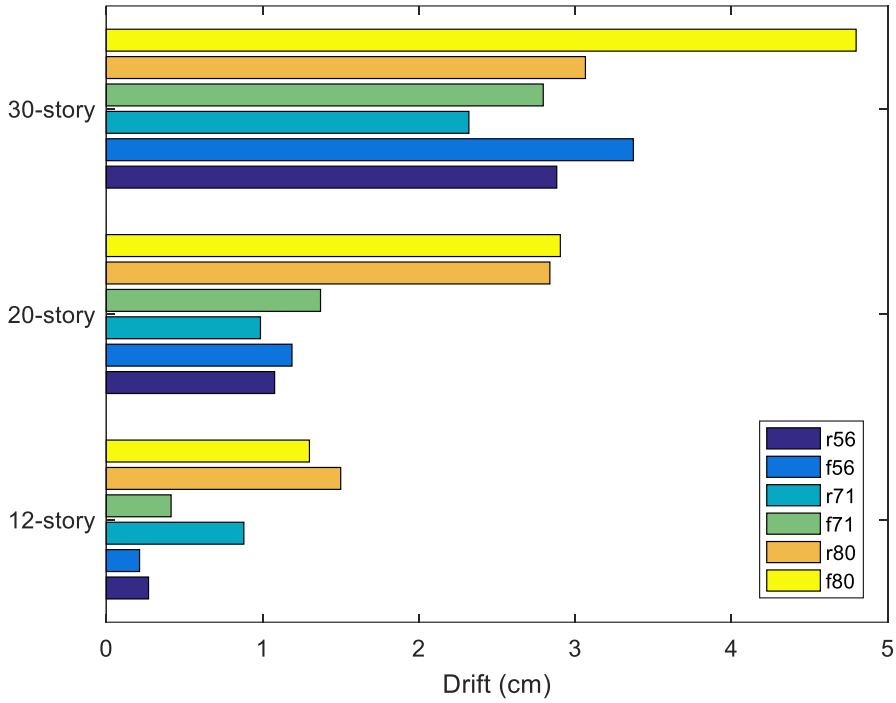

Figure 18: Maximum inter-story drift in the optimal diagrid models

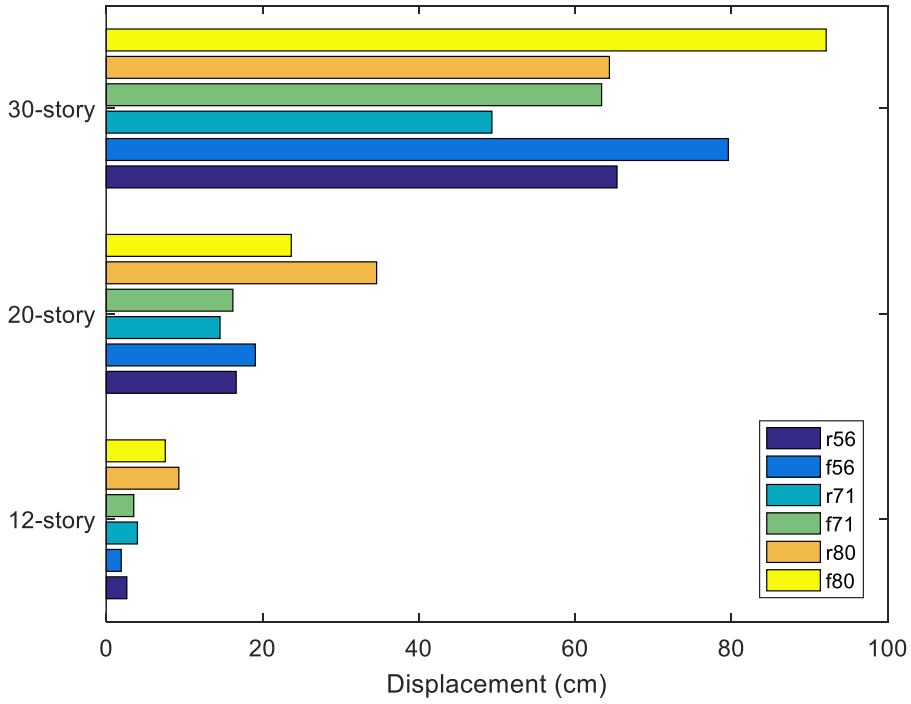

Figure 19: Maximum lateral displacement in the optimal diagrid models

[DOI: 10.22068/ijoce.2024.14.4.605]

6. CONCLUSION

In the present work, the structural weight was minimized subject to LRFD constraints on axial, flexural and shear behavior of all frame and diagonal elements of diagrid models. A variant of Falcon optimization algorithm was utilized to deal with practical section indices as discrete design variables to ensure that no approximation of structural properties affects the optimization results.

The design examples covered variation in diagrid geometry, its height and boundary condition regarding the effect of soil flexibility beneath the foundation. The angle of diagonal members with the horizontal line governs the diagrid geometry variation as the story height and bay length are fixed. According to the numerical results, the diagrid geometry has considerable effect on its optimal sizing design as well as the search space cardinality. Such a cardinality varied from to among the treated models. Proper convergence of the optimal process in such large-scale discrete problem was observed via histories of the global-best objective function.

In conclusion, the present study reveals how different angles in regular diagrids can change its optimal design against lateral forces such as wind loading in addition to gravitational loads. The effect of considering the soil flexibility beneath the foundations, depends on the diagrid angle and also its number of stories. For the regular diagrids of the present work, the angle was uniform among the structural height that brings about ease of practical design and fabrication. It is noted that the presented results are reliable for the employed design method and assumptions on the wind loading and soil conditions. More rigorous study of soil-structure interaction by nonlinear analyses and variation among the bays and stories of the diagrid structure will be of course a future scope of work.

REFERENCES

1. Ali MM, Moon KS. Structural Developments in Tall Buildings: Current Trends and Future Prospects. *Archit Sci Rev*. 2007;**50**:205–23.
2. Moon KS. Optimal grid geometry of diagrid structures for tall buildings. *Archit Sci Rev*. 2008;**51**:239–51.
3. Shahrouzi M, Meshkat-dini A, Azizi A. Simultaneous geometry and size optimization of diagrids against equivalent wind loading. Adv. Environ. Mater. Res. ACEM16, Jeju, South Korea, 31Aug-1Sep: Techno-Press; 2016.
4. Kaveh A, Shahrouzi M. Simultaneous topology and size optimization of structures by genetic algorithm using minimal length chromosome. *Eng Comput*. 2006;**23**:644–74.
5. Kaveh A, Shahrouzi M. An efficient stochastic search with minimal intial population for structural optimization. *Asian J Civ Eng*. 2010;**11**:741–62.
6. Molina D, Poyatos J, Ser J Del, García S, Hussain A, Herrera F. Comprehensive Taxonomies of Nature- and Bio-inspired Optimization: Inspiration Versus Algorithmic Behavior, Critical Analysis Recommendations. *Cognit Comput*. 2020;**12**:897–939.
7. Hussain K, Mohd Salleh MN, Cheng S, Shi Y. Metaheuristic research: a comprehensive survey. *Artif Intell Rev*. 2019;**52**:2191–233.
8. Kaveh A., Advances in Metaheuristic Algorithms for Optimal Design of Structures, Springer International Publishing, Switzerland, 3rd edition, 2021.

[DOI: 10.22068/ijoce.2024.14.4.605]

9 Kaveh A. Improved cycle basis for the flexibility analysis of structures, Computer Methods in Applied Mechanics and Engineering, 9(1976)267-72.
10. Shahrouzi M, Pashaei M. Stochastic Directional Search : an efficient heuristic for structural optimization of building frames. *Sci Iran*. 2013;**20**:1124–32.
11. Shahrouzi M. Optimal Spectral Matching of Strong Ground Motion by Opposition-Switching Search. EngOpt 2018 Proc. 6th Int. Conf. Eng. Optim., Lisbon, Purtugal: Springer International Publishing; 2018, p. 713–24.
12. Dokeroglu T, Sevinc E, Kucukyilmaz T, Cosar A. A survey on new generation metaheuristic algorithms. *Comput Ind Eng*. 2019;**137**:106040.
13. Holland JH. Genetic algorithms. *Sci Am*. 1992;**267**:66–72.
14. Rahami H, Kaveh A, Aslani M, Asl RN. A hybrid modified genetic-nelder mead simplex algorithm for large-scale truss optimization. *Int J Optim Civ Eng*. 2011;**1**:29–46.
15. Kaveh A, Rahami H, Shojaei I. *Swift Analysis of Civil Engineering Structures Using Graph Theory Methods*. Gewerbestrasse 11, 6330 Cham: Springer Nature Switzerland AG; 2020.
16. Kennedy J, Eberhart RC. *Swarm intelligence*. 2001.
17. Kaveh A, Talatahari S. A novel heuristic optimization method: Charged system search. *Acta Mech*. 2010;**213**:267–89.
18. Dorigo M. The Ant Colony Optimization Metaheuristic : 2001:1–42.
19. Shahrouzi M, Rahemi AA. Improved seismic design of structural frames by optimization of equivalent lateral load pattern. *Int J Civ Eng*. 2014;**12**:256–67.
20. Shahrouzi M, Emamzadeh S, Naserifar Y. A hybrid Simulated Annealing, Particle Swarm and Ant Colony Optimization for Design of Double-Curved Dams. *Int J Optim Civ Eng*. 2023;**13**:413–38.
21. Kaveh A, Farhoodi N. Layout optimization for x-bracing of planar steel frames using ant system. *Int J Civ Eng*. 2010;**8**:256–75.
22. Gholizadeh S, Poorhoseini H. Seismic layout optimization of steel braced frames by an improved dolphin echolocation algorithm. *Struct Multidiscip Optim*. 2016;**54**:1011–29.
23. Yang XS, He X. Bat algorithm: literature review and applications. *Int J Bio-Inspired Comput*. 2013;**5**:141.
24. Kaveh A, Bakhshpoori T. A new metaheuristic for continuous structural optimization: water evaporation optimization. *Struct Multidiscip Optim*. 2016;**54**:23–43.
25. Kaveh A, Ilchi Ghazaan M. A new meta-heuristic algorithm : vibrating particles system. *Sci Iran*. 2017;**24**:1–32.
26. Pierezan J, Coelho L. Coyote Optimization Algorithm: A New Metaheuristic for Global Optimization Problems. 2018 IEEE Congr. Evol. Comput., IEEE; 2018, p. 1–8.
27. Mirjalili S-A, Gandomi AH, Mirjalili SZ, Saremi S, Faris H, Mirjalili SM. Salp Swarm Algorithm: A bio-inspired optimizer for engineering design problems. *Adv Eng Softw*. 2017;**114**:163–91.
28. Vasconcelos Segundo EH de, Mariani VC, Coelho L. Design of heat exchangers using Falcon Optimization Algorithm. *Appl Therm Eng*. 2019;**156**:119–44.
29. Kaveh A, Zaerreza A. Shuffled shepherd optimization method: a new Meta-heuristic algorithm. *Eng Comput (Swansea, Wales)*. 2020;**37**:2357–89.
30. Kaveh A, Zaerreza A. *Structural Optimization Using Shuffled Shepherd Meta-Heuristic Algorithm: Extensions and Applications*. vol. 463. Cham: Springer Nature Switzerland; 2023.
31. Shahrouzi M, Kaveh A. An efficient derivative-free optimization algorithm inspired by

[DOI: 10.22068/ijoce.2024.14.4.605]

avian life-saving manoeuvres. *J Comput Sci*. 2022;**57**:101483.
32. Lee KS, Geem ZW. A new structural optimization method based on the harmony search algorithm. *Comput Struct*. 2004;**82**:781–98.
33. Geem ZW. *Music-inspired harmony search algorithm: theory and applications*. Berlin: Springer-Verlag; 2009.
34. Shahrouzi M, Naserifar Y. An Efficient Hybrid Particle Swarm and Teaching-Learning-Based Optimization for Arch-Dam Shape Design. *Struct Eng Int*. 2023;**33**:640–58.
35. Sadollah A, Bahreininejad A, Eskandar H, Hamdi M. Mine blast algorithm: A new population based algorithm for solving constrained engineering optimization problems. *Appl Soft Comput*. 2013;**13**:2592–612.
36. Gerasimidis S, Pantidis P, Knickle B, Moon KS. Diagrid Structural System for High-Rise Buildings: Applications of a Simple Stiffness-based Optimized Design. *Int J High-Rise Build*. 2016;**5**:319–26.
37. Tomei V, Imbimbo M, Mele E. Optimization of structural patterns for tall buildings: The case of diagrid. *Eng Struct*. 2018;**171**:280–97.
38. Bruggi M. Conceptual Design of Diagrids and Hexagrids by Distribution of Lattice Structures. *Front Built Environ*. 2020;**6**.
39. Montuori GM, Mele E, Brandonisio G, De Luca A. Geometrical patterns for diagrid buildings: Exploring alternative design strategies from the structural point of view. *Eng Struct*. 2014;**71**:112–27.
40. INBC:Part-10. *Iranian National Building Code, Part-10: Design of Steel Structures*. 4th ed. Tehran: Roads, Housing and Urban Development of Iran; 2013.
41. AISC. *AISC Manual of Steel Construction: Load and Resistant Design Factor*. Chicago, Illinois: American Institute of Steel Constuction; 2005.
42. Tucker VA. Gliding flight: speed and acceleration of ideal falcons during diving and pull out. *J Exp Biol*. 1998;**201**:403–14.
43. Yang X-S, Deb S. Eagle strategy using l´evy walk and firefly algorithms for stochastic optimization. *Springer Nat Inspired Coop Strateg Optim*. 2010:101–11.
44. Heidari A, Mirjalili S-A, Faris H, Aljarah I, Mafarja M, Chen H. Harris hawks optimization: Algorithm and applications. *Futur Gener Comput Syst*. 2019;**97**:849–72.
45. Tucker VA, Tucker AE, Akers K, Enderson JH. Curved flight paths and sideways vision in peregrine falcons (Falco peregrinus). *J Exp Biol*. 2000;**203**:3755–63.
46. Kaveh A., The application of topology and metroid theory to the analysis of structures, PhD thesis, Imperial College, University of London, 1974.
47. INBC:Part-6. *Iranian National Building Code, Part-6: Loading on Structures*. 4th ed. Tehran: Roads, Housing and Urban Development of Iran; 2013.
48. Mylonakis G, Nikolaou S, Gazetas G. Footings under seismic loading: Analysis and design issues with emphasis on bridge foundations. *Soil Dyn Earthq Eng*. 2006;**26**:824–53.

[DOI: 10.22068/ijoce.2024.14.4.605]